Published OnlineFirst September 9, 2019; DOI: 10.1158/1535-7163.MCT-18-1380

Small Molecule Therapeutics

Molecular Cancer Therapeutics

CNDAC-Induced DNA Double-Strand Breaks Cause Aberrant Mitosis Prior to Cell Death

Xiaojun Liu[1], Yingjun Jiang[1], Kei-ichi Takata[2], Billie Nowak[1], Chaomei Liu[1], Richard D. Wood[2], Walter N. Hittelman[1], and William Plunkett[1,3]

Abstract

Incorporation of the clinically active deoxycytidine analogue 2′-*C*-cyano-2′-deoxy-1-β-D-arabino-pentofuranosyl-cytosine (CNDAC) into DNA generates single-strand breaks that are subsequently converted to double-strand breaks (DSB). Here, we investigated the cellular manifestations of these breaks that link these mechanisms to cell death, and we further tested the relevance of DNA repair pathways in protection of cells against CNDAC damage. The present investigations demonstrate that following exposure to CNDAC and a wash into drug-free medium, chromosomal aberrations, DNA strand breaks, and multinucleate cells arose. These portended loss of viability and were dependent upon exposure time, CNDAC concentration, and passage through mitosis. Following a pulse incubation with CNDAC, live cell imaging using GFP-tagged histone H2B as a marker demonstrated a normal rate of progression to mitosis, but a concentration-dependent delay in passage to a second mitosis. Progression through mitosis was also delayed and accompanied by formation of multinucleate cells. CNDAC-treated cells lacking XPF-ERCC1 nuclease function showed a 16-fold increase in chromosome aberrations. Chromosomal damage in *Rad51D*-mutant cells (homologous recombination repair deficient) were even more severely affected with extensive aberrations. Rodent or human *Polq* (*POLQ*) mutant cells, defective in Pol θ–mediated alternative end joining, did not show enhanced cellular sensitivity to CNDAC. These findings are consistent with formation of DSBs in the second S-phase following exposure, resulting in chromosome aberrations, aberrant mitoses, and subsequent apoptosis.

Introduction

The nucleoside analogue 2′-C-cyano-2′-deoxy-1-β-D-arabino-pentofuranosyl-cytosine (CNDAC) and its orally bioavailable prodrug sapacitabine are currently undergoing clinical trials for acute myeloid leukemia (AML) and myelodysplastic syndromes (1–4). CNDAC has a mechanism of action that is distinct from other deoxycytidine analogs (5). After phosphorylation to the triphosphate and its incorporation into DNA, the instability of the analogue induces a β-elimination rearrangement that results in the transformation of the analogue to CNddC, a *de facto* 3′-terminus DNA chain terminator (6, 7). The resulting single-strand breaks (SSB) have been shown to be converted into double-strand breaks (DSB) during DNA replication in a subsequent S-phase (8). These consequences are supported by evidence of chromosome damage.

The molecular mechanism(s) of action of CNDAC have been investigated by employing cell lines process blocked 3′ ends lead to increased sensitivity to CNDAC. Exposure of cells with defective XPF-ERCC1 nuclease to CNDAC for one cell cycle decreased the IC_{50} in clonogenic assays by 3- to 5-fold (9). In addition, the viability of cells lacking tyrosyl-DNA phosphodiesterase 1 (TDP1) was similarly sensitized to CNDAC, consistent with the conclusion that it also can remove a CNddC-terminated DNA end (10). In contrast, the viability of cells lacking either base excision repair function or DNA mismatch repair was not changed from those with intact repair pathways.

The nature of the DNA damage initially reported indicated the presence of DSBs. Treatment of cells lacking any of several enzymes (ATM, XRCC3, RAD51D, BRCA2) in the ATM-dependent homologous recombination pathway (HR) with CNDAC for two cell cycle times decreased IC_{50} for clonogenicity by 30- to 100-fold (8). The finding that the viability of cells lacking nonhomologous end-joining (NHEJ) function was not diminished beyond that of NHEJ-competent cells supported the conclusion that HR repair of CNDAC-induced DSB is the primary mechanism of cell death (8). However, an alternative end-joining pathway, also known as microhomology-mediated end joining, has recently emerged as an important repair mechanism complementary to the classical NHEJ pathway (11). DNA polymerase θ (Pol θ) is a key component involved in alternative end-joining and has been shown to be synthetic lethal with the HR pathway (12, 13). The possible contribution of this pathway to repair of CNDAC-induced damage has not yet been reported.

At the subcellular level, CNDAC exposure gives rise to chromosomal aberrations (14). However, it remains obscure as to

[1]Department of Experimental Therapeutics, The University of Texas MD Anderson Cancer Center, Houston, Texas. [2]Department of Epigenetics and Molecular Carcinogenesis, The University of Texas MD Anderson Cancer Center, Houston, Texas. [3]Department of Leukemia, The University of Texas MD Anderson Cancer Center, Houston, Texas.

Note: Supplementary data for this article are available at Molecular Cancer Therapeutics Online (http://mct.aacrjournals.org/).

Current address for K. Takata: Center for Genomic Integrity, Institute for Basic Science, Ulsan 44919, Republic of Korea.

Current address for X. Liu: School of Health Professions, The University of Texas MD Anderson Cancer Center, Houston, TX.

Corresponding Author: William Plunkett, The University of Texas MD Anderson Cancer Center, 1901 East Road, Houston, TX 77054. Phone: 713-792-3335; E-mail: wplunket@mdanderson.org

Mol Cancer Ther 2019;18:2283–95

doi: 10.1158/1535-7163.MCT-18-1380

Published OnlineFirst September 9, 2019; DOI: 10.1158/1535-7163.MCT-18-1380

how CNDAC-induced DSBs, manifested as chromosomal damage, lead to cell death. In the current study, we focused on CNDAC-caused DNA lesions at the chromosomal level. Chinese hamster ovary (CHO) cell lines deficient in either XPF (a component of the XPF-ERCC1 nuclease) or RAD51D (a component of the HR pathway) were investigated. In addition to chromosomal aberrations, we observed that cells treated with CNDAC formed multiple nuclei, a prominent feature associated with mitotic catastrophe. To better characterize the events before, during and after the aberrant mitosis, we used live cell imaging to track cell fate in real time.

Materials and Methods

Materials

The nucleoside analogue CNDAC was synthesized as described and generously provided by Professor A. Matsuda (University of Sapporo, Hokkaido, Japan; refs. 15, 16). The following reagents were purchased from Thermo Fisher Scientific: Karyomax Giemsa stain stock solution (catalog no. #10092013); Gurr buffer solution tablets (catalog no. #10582013); Histomount mounting solution (catalog no. #008030); OptiMEM I reduced serum medium (catalog no. #31985062); Blasticidin S HCl solution (catalog no. #A1113903). Sources of other reagents are listed as follows: Accutase (catalog no. #07920) from Stemcell Technologies; pBOS-H2BGFP vector (catalog no. #559241) from BD Pharmingen; FuGENE HD transfection reagent (catalog no. #E23110) from Promega; protease inhibitor cocktail tablets (catalog no. #04693159001) and phosphatase inhibitor cocktail tablets (catalog no. #04906837001) from Roche.

Antibodies

mAbs to phospho-Ser1981 ATM (catalog no. #05-740) and phospho-Ser139 H2AX (catalog no. #05-636) were purchased from Upstate/Millipore. Rabbit mAb to DNA-PKcs (catalog no. #ab32566) and polyclonal antibody to ATM (catalog no. #ab17995) were from Abcam. Polyclonal antibody to H2AX (catalog no. #GTX108272) was from GeneTex. α-Tubulin and β-actin mAbs were from Sigma-Aldrich (catalog no. #T5168). mAb to PARP (catalog no. #51-6639GR) was from BD Pharmingen. mAb to caspase-3 (catalog no. #3004) was from BioVision, and polyclonal antibody to cleaved caspase-3 (catalog no. #9661) was from Cell Signaling Technology.

Cell lines

CHO lines AA8 [wild type (WT)] and UV41 (*Xpf* mutant) were purchased from the ATCC. The AA8-derived *Rad51D* knockout line, 51D1, and the *Rad51D* complemented line, 51D1.3 (17), were gifts from Dr. L. Thompson (Lawrence Livermore National Laboratory, Livermore, CA). All CHO lines were grown in αMEM (free of ribonucleosides and deoxyribonucleosides) supplemented with 10% heat-inactivated FBS and GlutaMax. Mouse embryonic fibroblast (MEF) lines $Polq^{+/+}$ (55-5 Tag), $Polq^{+/-}$ (55-7 Tag), and $Polq^{-/-}$ (55-6 Tag; ref. 11) were cultured in DMEM supplemented with 10% heat-inactivated FBS and GlutaMax. Human osteosarcoma U2OS $POLQ^{+/+}$ cell lines were used by RDW and KT to generate two independent $POLQ^{-/-}$ knockout clones F10 and G6. The U2OS cells were cultured in the same medium as the MEFs. *POLQ* knockout by frameshift was confirmed by genomic DNA sequencing and reduced *POLQ* mRNA level was verified by qPCR (Supplementary Fig. S3C). $POLQ^{+/+}$, $POLQ^{-/-}$, (F10) and $POLQ^{-/-}$ (G6) were stably transfected with shControl and shDNA-PKcs, respectively. Knockdown of DNA-PKcs was confirmed by immunoblotting. The human lung cancer cell line H460 was a gift from David G. Beer (University of Michigan, Ann Arbor, MI). All human cell lines were authenticated using short tandem repeat DNA fingerprinting by the Characterized Cell Line Core at the MD Anderson Cancer Center (Houston, TX). All rodent and human cells were free of *Mycoplasma*, as certified by the same core facility using the MycoAlert Kit from Lonza. Each line was used in experiments for no more than 15 passages after recovering from frozen seed stocks that were authenticated prior to freezing.

Cell-cycle analysis

Adherent cells were detached with Accutase, washed with ice-cold PBS (pH 7.4), and fixed in 70% ethanol for at least 1 hour on ice or overnight at 4°C. Fixed cells were washed with PBS and incubated with 50 μg/mL propidium iodide (PI) and 2.5 μg/mL DNase-free RNase (14). A Becton Dickinson FACSCalibur flow cytometer with BD CellQuest Pro program was used to determine the DNA content in each sample by measuring the fluorescence from at least 20,000 cells.

Apoptosis analysis

Detached cells were washed with PBS and resuspended in 100 μL of binding buffer with 5 μL of Cy5-conjugated Annexin V (BD Pharmingen, catalog no. #559934). After 15-minute incubation in the dark at room temperature, 400 μL of binding buffer with 5 μL of 50 μg/mL PI was added to each sample. At least 20,000 cells were analyzed using a BD FACSCalibur flow cytometer with the CellQuest Pro software. Cells stained positive for Annexin V (PI negative and positive) were considered apoptotic cells.

Cell growth rate analysis

Exponentially growing cells were plated in multiple 100-mm dishes at 10^5/dish. At indicated times, duplicate dishes of cells were detached using 0.05% trypsin–EDTA solution and subjected to quantitation of total cell numbers using a Coulter Counter (Beckman Coulter Life Sciences). The total number of cells (mean of two dishes) were plotted as a function of time. Population doubling time (PDT) of each cell line was computed using the tool at http://www.doubling-time.com/compute_more.php.

Clonogenic survival assay

Adherent MEF or human U2OS cells, WT or *Polq* (or *POLQ*) knockout, were seeded in 6-well plates one day before they were exposed to a range of concentrations of drugs for 24 hours. Cells were washed into drug-free medium and incubated for an additional 3 days (MEFs) or 6 days (U2OS lines) to form colonies. Colonies in triplicate wells were fixed and stained with crystal violet/ethanol and counted under a dissecting microscope (cutoff $\geq$ 50 cells) or scored electronically (GelCount, Oxford Optronix). Percent survival is expressed as mean ± SD.

Cytogenetic analysis

Colcemid (100 ng/mL) was added to cell cultures before harvesting. Mitotic spreads were prepared as described previously (14). A minimum of 50 metaphase spreads were analyzed for each sample by the T.C. Hsu Molecular Cytogenetics Core at the MD Anderson Cancer Center.

Published OnlineFirst September 9, 2019; DOI: 10.1158/1535-7163.MCT-18-1380

Detection of multinucleate cells

CNDAC-treated AA8 cells were detached with Accutase, transferred onto slides using a Shandon Cytospin 3 cytocentrifuge (700 rpm for 5 minutes at room temperature), and air dried briefly. Cells were fixed in 70% ethanol at 4°C for a minimum of 1 hour and air dried again. Giemsa stain solution was freshly diluted in Gurr buffer (1 tablet in 1 L of water, pH 6.8) to 4% (v/v) and used for staining the cells on slides for 20 minutes at room temperature. Cells were rinsed, air dried overnight, and mounted with coverslips using Histomount mounting solution. Images of cells in bright field were captured at randomly selected fields under a Nikon light microscope (20× objective lens) using a Sony 3CCD color video camera (model no. DXC-390, SimplePCI software). For each treatment, nuclear morphology of a minimum of 400 cells was analyzed and categorized according to the samples in Supplementary Fig. S4. Qualitative images were taken using 40× and 100× oil lenses.

Immunoblotting

Cell lysates, prepared by sonication in RIPA buffer supplemented with protease inhibitor and phosphatase inhibitor cocktail tablets, were loaded on Bis-Tris 4% to 12% polyacrylamide gradient gels (Bio-Rad) and transferred onto nitrocellulose membranes (0.22 μm) as described previously (14). Immunoblots were visualized and target bands were quantitated by Li-Cor Odyssey Version 4.0 software.

Single-cell gel electrophoresis (comet assay)

DNA strand breaks were detected using single-cell gel electrophoresis under both neutral pH and alkaline conditions using CometAssay Electrophoresis System II (Trevigen, catalog no. #4250-050-ES). After electrophoresis, cells embedded in low-melting agarose (comets) were fixed with 70% ethanol and stained with SYBR Gold (Thermo Fisher Scientific, catalog no. #S-11494). Images of comets in random fields were captured under Olympus IX70 inverted fluorescence microscope using Olympus DP70 CCD camera and 4× objective, and subjected to quantitation using Comet Assay IV software (Instem). At least 200 cells per treatment condition were scored. An increase in Olive tail moment from a neutral comet assay was used as a readout for DSBs, whereas that from an alkaline comet assay for the sum of SSBs and DSBs. Additional images were taken using 10× or 20× objectives to feature more details of comets.

Stable expression of histone H2B-GFP

AA8 cells were transfected with pBOS-H2BGFP vector (18) using FuGENE transfection reagent in OptiMEM I. Cells stably expressing H2B-GFP fusion proteins were selected by addition of 5 μg/mL blasticidin in complete medium over a period of 2 to 3 weeks. Cultures were monitored daily under Olympus IX70 inverted fluorescent microscope and imaged as needed using 20× objective at both fluorescent and bright light channels. GFP-positive cells were isolated on BD FACS Aria IIu cell sorter and two populations, GPF^+ high and GFP^+ low, were collected and propagated separately. No significant difference in growth rate, based on size of colonies formed, was observed for the two populations. The GFP^+ high cells were used for live cell imaging. H460 cells were stably transfected with pBOS-H2BGFP vector following the same procedure as AA8.

Time-lapse video microscopy

AA8/H2B-GFP cells were grown in chamber slides overnight and set up in an Olympus live cell imaging station enclosed by a micro cell incubator with humidified air and active controllers for temperature (37°C) and CO_2 (5%). HEPES (10 mmol/L) was supplemented in complete medium to increase pH buffering capacity. A 20× relief phase contrast objective was used on the Olympus microscope. Multiple positions were randomly selected with well isolated cells at a low density and the objective was adjusted to focus for each position. Cells were exposed to CNDAC at 0.5, 1, and 10 μmol/L, respectively, for 6 hours before washout. The microscope and connected computer were programed to capture images of both GFP fluorescence and bright field every 15 minutes after CNDAC washout. The live cell imaging was carried out for 114 hours after the initial 63 hours. Meta Morph Advanced image analysis software was applied to compile images into time-lapse videos and perform subsequent analyses.

Statistical analysis

For the quantitation of chromosomal aberrations, tail moment of comets, and the live cell imaging, intergroup comparisons of endpoints in response to various treatments were made using a *t* test with two-tailed distribution and two-sample unequal variance in Excel.

Results

Deficiency in XPF results in greater levels of chromosomal aberrations induced by CNDAC

Cellular response to CNDAC is concentration- and time-dependent (14). We postulated that processing or DNA replication across the unrepaired nicks would generate DSBs, which in turn would lead to the death of cells by yet undefined mechanism (s). To address this, cytogenetic endpoints were used to characterize the consequences of deficiencies in specific DNA repair mechanisms. Metaphase chromosomal aberrations (including breaks and gaps) were compared in the WT AA8 line and its mutant UV41, which lacks XPF (19, 20). The cell lines were continuously treated with CNDAC at 1 μmol/L, which is a non-arresting concentration for both lines after one cell cycle (15–16 hours). However, after drug exposure for 2 cell cycles (30 hours), the mutant line was delayed in transiting the second G2, whereas this was not observed for the WT cells (Supplementary Fig. S1). Therefore, the addition of colcemid was scheduled earlier than for WT cells to ensure prolonged incubation time to enrich the number of mitotic cells for analysis. In cells lacking XPF, chromosomal aberrations increased from an average of 0.4/metaphase to 0.9/metaphase after one cell cycle treatment with 1 μmol/L CNDAC, and to 5.6/metaphase after two cell cycles, that is, 30 hours (Fig. 1A, gray bars, $n \geq 60$, $P < 0.01$; Fig. 1B). Chromosomal aberrations in the WT cells did not increase as dramatically, from 0.05/metaphase to 0.2/metaphase after two cell cycles (Fig. 1A, black bars, $n \geq 55$, $P < 0.05$). These data support the interpretation that SSBs induced by CNDAC in the first S-phase can be converted into DSBs during the second S-phase when replication forks encounter unrepaired SSBs and that an XPF-dependent mechanism provides protection against generation of DSBs.

The increase in chromosomal aberrations after CNDAC exposure, regardless of length of time, was greater in UV41 cells compared to the WT. The mean values of chromosomal

Published OnlineFirst September 9, 2019; DOI: 10.1158/1535-7163.MCT-18-1380

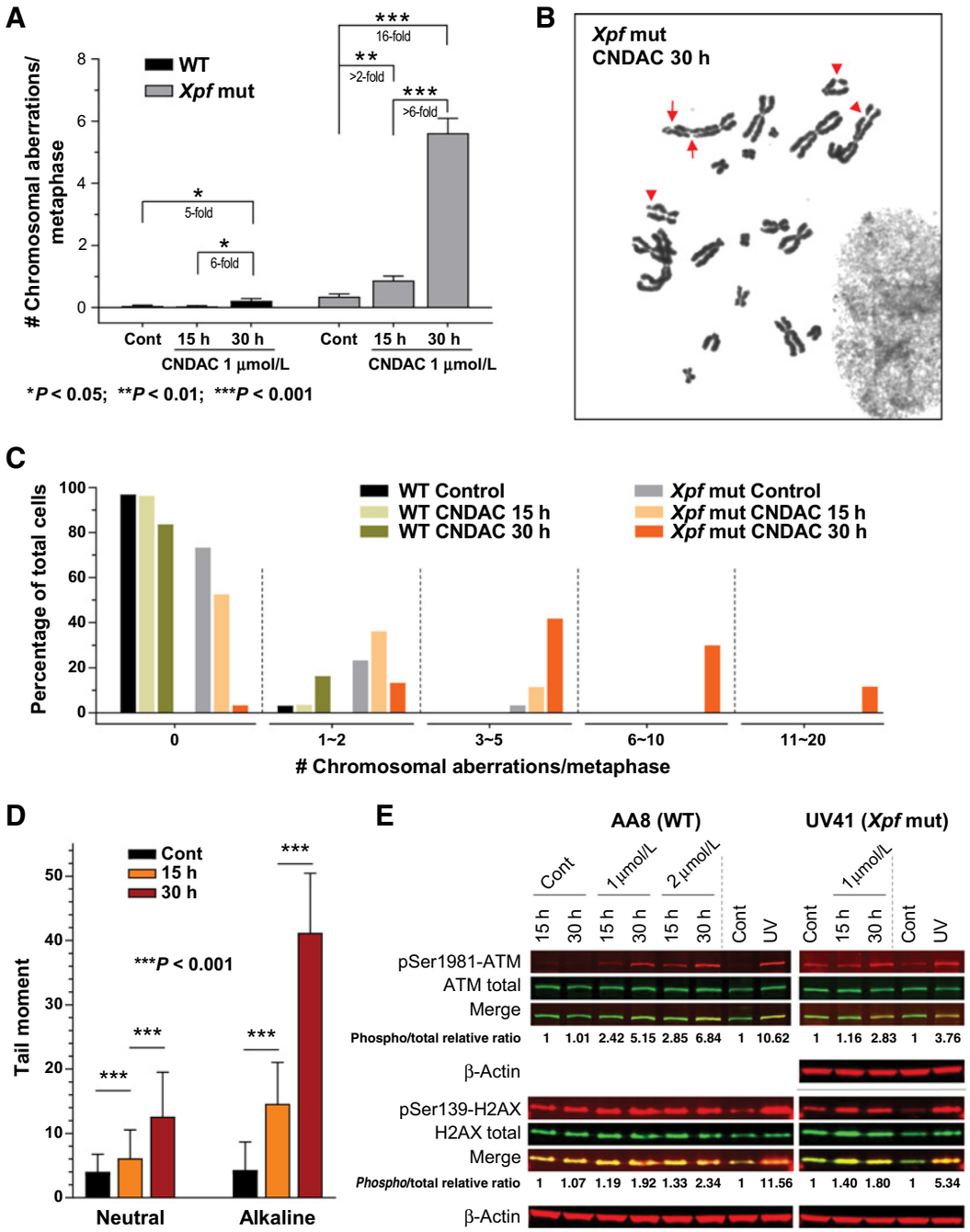

Figure 1.

Increased chromosomal aberrations in XPF-deficient cells after CNDAC treatment. Wild-type AA8 cells and UV41 (*Xpf* mutant) cells were treated with 1 μmol/L CNDAC for 15 and 30 hours. **A,** Quantitative plot of chromosomal aberrations (gaps and breaks) in both WT and XPF-mutant cell lines. Bars show mean ± SD values of numbers of chromosomal aberrations per metaphase. **B,** Representative metaphase image of *Xpf*-mutant cells treated with 1 μmol/L CNDAC for 30 hours. An arrow indicates a gap (short) or a break (long). **C,** Bar plot showing distribution of chromosomal aberrations in both cell lines. More than 2 chromosomal aberrations/metaphase were not detected in WT control or CNDAC-treated cells. **D,** Bar plot showing comet tail moment of *Xpf*-mutant cells treated with 1 μmol/L CNDAC for 15 and 30 hours, respectively, from comet assays under neutral and alkaline conditions. For each treatment, 200 cells were quantified and the mean ± SD values of tail moment were presented. **E,** Immunoblotting of phospho- and total ATM and H2AX in WT and *Xpf*-mutant cells treated with CNDAC at indicated concentrations for 15 and 30 hours. The ratios of phospho- to total proteins were calculated and normalized to those of corresponding controls. Each cell line was exposed to 50 J/m^2 UV irradiation and incubated for 30 minutes before being collected to use as a positive control for the phosphorylation of ATM or H2AX. β-Actin was used as a loading control.

Published OnlineFirst September 9, 2019; DOI: 10.1158/1535-7163.MCT-18-1380

aberrations increased 6-fold in WT and >6-fold in XPF-mutant cells after two PDTs compared with those treated for only one PDT (Fig. 1A, 30- vs. 15-hour bars). More impressively, the average number of chromosomal aberrations increased 16-fold after two cell cycles in the mutant (5.6 aberrations/metaphase) compared with a 5-fold change in the WT cells (0.22/metaphase, Fig. 1A). The distribution of chromosomal aberration frequencies was also distinct between the two lines. Sixteen percent of WT cells treated with CNDAC for two PDTs had 1 to 2 chromosomal aberrations, and no cells had more than 2 aberrations per metaphase. In contrast, 42%, 30%, and 12% of XPF-mutant cells exhibited 3–5, 6–10, and 10–20 aberrations per metaphase, respectively (Fig. 1C). These results are consistent with a decrease in clonogenic survival in XPF-deficient cells after CNDAC exposure (9), indicating that XPF contributes to the repair of CNDAC-induced damage.

To provide direct evidence for the presence of DNA strand breaks, comet assays were performed in XPF-deficient and WT cells. In XPF-mutant cells, both neutral and alkaline comet assays demonstrated significant elevation in tail moments after CNDAC incubation (Fig. 1D). Under a neutral condition, the tail moment of control cells increased from 4.06 ± 2.72 to 6.12 ± 4.47 after incubation with 1 μmol/L CNDAC for 15 hours, and further to 12.61 ± 6.92 at 30 hours (Fig. 1D; Supplementary Fig. S2A). This result parallels the change in chromosomal aberrations after CNDAC treatment (Fig. 1A). The minor increase in either comets or chromosomal aberrations after 15-hour CNDAC exposure could be interpreted as the conversion of endogenous SSBs into DSBs upon CNDAC incorporation during the first cell cycle. Both comets and chromosomal aberrations soared after 30-hr incubation with CNDAC, indicating an increase in DSBs after a second cell cycle. The comet assay under an alkaline condition revealed a similar change in comets but to a greater extent. The tail moment of untreated UV41 cells was 4.32 ± 4.36, while the CNDAC-treated cells presented a tail moment of 14.63 ± 6.44 at 15 hours and 41.2 ± 9.28 at 30 hours, respectively (Fig. 1D; Supplementary Fig. S2A). Furthermore, the phosphorylation of ATM on Ser1981 and H2AX on Ser139 (γ-H2AX) increased slightly at 15 hours and to a greater extent after 30 hours of CNDAC treatment (Fig. 1E, right). Together, the comet assays and immunoblot results in XPF-deficient cells demonstrated that CNDAC-induced SSBs could be transformed into DSBs after a second S-phase. Although the WT AA8 cells presented increased levels of phosphorylated ATM and H2AX in a similar pattern to that found in the XPF mutants (Fig. 1E, left), comet tails were not discernible under alkaline condition when AA8 cells were exposed to 2 μmol/L CNDAC for 30 hours (2 cycles). However, comet tail legnth greatly increased after 10 μmol/L CNDAC (Supplementary Fig. S2B and S2C). The tail moments of AA8 cells were 7.2 ± 6.4 for the control, 52.9 ± 7.0 after 15-hour treatment and 75.5 ± 10.7 after 30-hour treatment.

Rad51D-defective cells present severe chromosomal damage in response to CNDAC

HR is the main pathway to repair DSBs induced by CNDAC (8). Here, we compared the cytogenetic changes after CNDAC treatment in cells deficient in RAD51D, a component of the HR mechanism (21), and cells complemented with RAD51D. In the absence of CNDAC exposure, RAD51D-deficient cells had an elevated background of chromosome alterations. Seventy-three percent had no apparent spontaneous chromosomal alteration; 23.8% and 1.6% presented 1–2 and 3–4 breaks per metaphase, respectively; the remaining 1.6% had fusions (Fig. 2A, gray bars, $n = 63$). In untreated RAD51D complemented cells, no aberrations were detected in 90% of the population, and 1–2 aberrations per metaphase were seen in the remainder of cells (Fig. 2A, black bars, $n = 80$). These data show a baseline genetic instability that can be attributed to deficiency in RAD51D.

A larger portion of the RAD51D complemented cells (Fig. 2A, 19%, $n = 99$) bore 1–2 chromosomal breaks, when exposed to 1 μmol/L CNDAC for two PDTs, than those exposed to CNDAC for only one population doubling time (Fig. 2A, 8.3%, $n = 72$). At both times, a minor portion of cells treated with CNDAC (1%–2%) had more than 2 breaks per metaphase. Notably, after two cell cycles, 99% of all metaphases from CNDAC-treated RAD51D complemented cells could be analyzed, including 78% metaphases free of aberration and only 1% was unscorable (Fig. 2A, $n = 99$). In contrast, 76% of the metaphases in RAD51D-deficient cells exposed to CNDAC for two PDTs had severe chromosomal damage and therefore were unscorable for individual aberrations (Fig. 2B). Radial formation was apparent in some chromosomes, consistent with a defect in the HR function. Another 9% and 2% presented 1–2 breaks and 3–4 breaks per metaphase, respectively. Only 13% of the population were free of chromosomal aberrations (Fig. 2A, $n = 106$). As for the RAD51D-deficient cells treated with CNDAC for one population doubling time, 28% and 3% had 1–2 breaks and 3–4 breaks per metaphase, respectively; 1.5% had fusions; and the rest were free of chromosomal aberration (Fig. 2A, $n = 68$). The RAD51D-deficient cells showed fewer aberrations after one cell cycle than that after two cell cycles. This is consistent with results from the RAD51D complemented cells and the paired XPF cells as well, further supporting the hypothesis that DSBs are formed during a second cell cycle. Importantly, the much greater extent of chromosome damage in cells exposed to CNDAC for a second S-phase relative to that in cells treated for only a single cell cycle is consistent with the much greater clonogenic sensitivity caused by defects in homologous recombination repair than by a defect in XPF-ERCC1 nuclease (8, 9).

Lack of DNA polymerase θ does not confer sensitivity to CNDAC

The role of the alternative DNA end-joining pathway in the repair of CNDAC-induced damage, if any, has not be defined. We compared the clonogenic survival rate of WT cells with a MEF line in which Pol θ, the product of the *Polq* gene, had been knocked out (11). The clonogenic survival of MEF cells that were either proficient or deficient in Pol θ was similar (Fig. 3A, $P = 0.051$). The PDTs of MEFs with different *Polq* status were 15.9 hours for $Polq^{+/+}$, 19.8 hours for $Polq^{+/-}$, and 25.5 hours for $Polq^{-/-}$ (Supplementary Fig. S3A). Consistent with the above observations, clonogenic assays of human U2OS $POLQ^{+/+}$ and $POLQ^{-/-}$ cells transfected with shControl were similarly sensitive to CNDAC (Fig. 3B, left), while $POLQ^{-/-}$ cells were sensitized about 2-fold to the comparator DNA strand-breaking agent, bleomycin (Fig. 3B, right). Previous investigations demonstrated that cells lacking the classical NHEJ component, DNA-PKcs, were not sensitized to CNDAC (8). Therefore, we investigated the CNDAC sensitivity of cells defective in both classical NHEJ and alternative end-joining. U2OS $POLQ^{+/+}$ and $POLQ^{-/-}$ cells stably transfected with shDNA-PKcs showed similar sensitivity to each

Published OnlineFirst September 9, 2019; DOI: 10.1158/1535-7163.MCT-18-1380

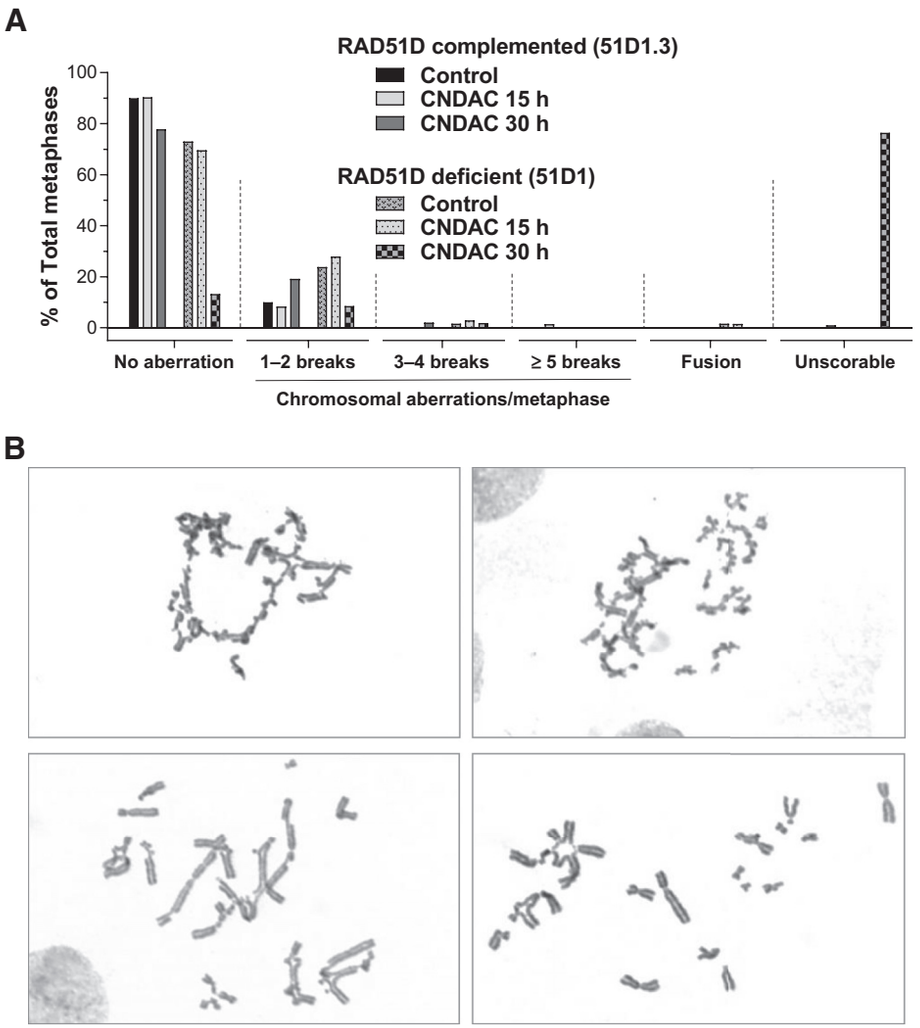

Figure 2.
Diverse cytogenetic changes in cells lacking RAD51D after CNDAC exposure. Wild-type AA8 cells and RAD51D-deficient cells (51D1) were treated with 1 μmol/L CNDAC for 15 and 30 hours, respectively. **A,** Bar plot showing percentage of cells with various types of chromosomal aberrations, including breaks, fusions, and unscorable metaphases, in both cell lines. **B,** Representative images of severe chromosomal damage induced by CNDAC (1 μmol/L, 30 hours) in RAD51D-deficient cells, 40× objective used.

agent in clonogenicity assays (Fig. 3C), although the PDT of *POLQ*$^{+/+}$ cells (27.0 hours) was somewhat more rapid relative to that of *POLQ*$^{-/-}$ cells (31.8 hours). However, the PDTs were further prolonged in DNA-PKcs knockdown *POLQ*$^{+/+}$ (41.2 hours) and *POLQ*$^{-/-}$ (46.1 hours) cells (Supplementary Fig. S3B). Therefore, depletion of Pol θ and/or DNA-PKcs in U2OS cells may hinder cell proliferation. Thus, similar findings in the two cell lines compromised for Pol θ function indicates that the alternative end-joining pathway is dispensable for repair of CNDAC-induced DSBs.

Exposure to CNDAC induces formation of multinucleate cells

CHO cells manifested metaphases with chromosomal aberrations in response to CNDAC to a greater extent after two PDTs and in the absence of key components of DNA damage repair pathways, such as XPF or RAD51D. To further study the consequences of entering mitosis with chromosomal instability, we analyzed the incidence of multinucleate formation following exposure to AA8 cells to CNDAC 24 hours. Because only WT cells were used in the study, a higher concentration of CNDAC (10 μmol/L, causing G_2 arrest) was tested in addition to two lower and nonarresting concentrations (0.5 and 1 μmol/L). Cells incubated with CNDAC for 24 hours were released into drug-free medium and analyzed for effects on their inability to complete normal mitosis as indicated by multinucleate formation after drug washout. Atypical interphase cells with more than a single nucleus were collectively counted as multinucleate (Supplementary Fig. S4C–S4G). The percentage of such cells increased in a CNDAC concentration-dependent fashion. Notably, among cells exposed to 1 μmol/L CNDAC, multinucleation was identified in approximately 22% and 13% of the population 24 and 48 hours after drug washout, respectively (Fig. 4A and B II). It was more evident that about 24% and 34% of 10 μmol/L CNDAC-treated cells presented multinucleation at 24 and 48 hours, respectively (Fig. 4A and B III-IV). When cells were exposed to CNDAC for 15 hours and then released in drug-free medium, a substantial increase in multinucleation was only observed in cells treated with 10 μmol/L CNDAC, not those with 0.5 or 1 μmol/L CNDAC (Supplementary Table S1). This is likely because longer drug-exposure time allows for more CNDAC incorporation in the DNA of all cells. Nevertheless, in both 24- and 15-hour schedules, multinucleation was not evident until after two PDTs, suggesting that the abnormal nuclear alterations occur after a second mitosis.

Published OnlineFirst September 9, 2019; DOI: 10.1158/1535-7163.MCT-18-1380

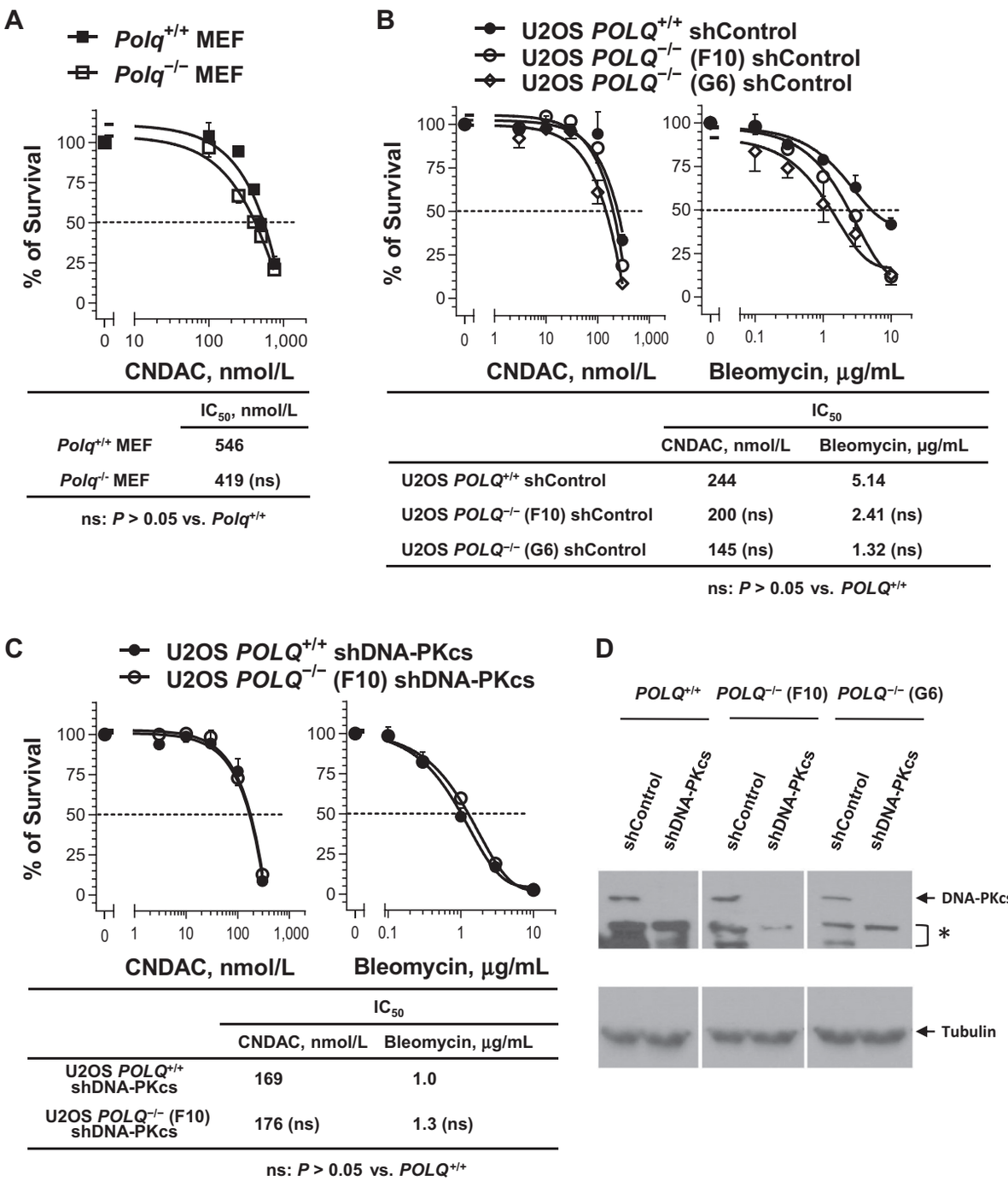

	IC_{50}, nmol/L
Polq$^{+/+}$ MEF	546
Polq$^{-/-}$ MEF	419 (ns)

ns: $P > 0.05$ vs. *Polq*$^{+/+}$

	IC_{50}	
	CNDAC, nmol/L	Bleomycin, μg/mL
U2OS *POLQ*$^{+/+}$ shControl	244	5.14
U2OS *POLQ*$^{-/-}$ (F10) shControl	200 (ns)	2.41 (ns)
U2OS *POLQ*$^{-/-}$ (G6) shControl	145 (ns)	1.32 (ns)

ns: $P > 0.05$ vs. *POLQ*$^{+/+}$

	IC_{50}	
	CNDAC, nmol/L	Bleomycin, μg/mL
U2OS *POLQ*$^{+/+}$ shDNA-PKcs	169	1.0
U2OS *POLQ*$^{-/-}$ (F10) shDNA-PKcs	176 (ns)	1.3 (ns)

ns: $P > 0.05$ vs. *POLQ*$^{+/+}$

Figure 3.

Clonogenic survival of human and mouse cell lines in response to CNDAC is independent of the status of DNA polymerase θ (*POLQ* or *Polq*) in the alternative end joining pathway. **A,** *Polq*$^{+/+}$ and *Polq*$^{-/-}$ MEF lines were treated with CNDAC for 24 hours and allowed to form colonies in the absence of CNDAC. **B,** *POLQ*$^{+/+}$ and *POLQ*$^{-/-}$ (clones F10 and G6) human osteosarcoma U2OS lines stably expressing shControl were treated with varying concentrations of CNDAC or bleomycin for 24 hours in colony formation assays. **C,** *POLQ*$^{+/+}$ and *POLQ*$^{-/-}$ U2OS lines stably expressing shDNA-PKcs were treated with CNDAC or bleomycin for 24 hours before washout for colony formation. Representative plots of percentage of cell survival as a function of drug concentration are shown. IC_{50} values of each agent are listed in the inserted table. "ns" stands for not significant. **D,** Immunoblotting of DNA-PKcs in *POLQ*$^{+/+}$ and *POLQ*$^{-/-}$ (clones F10 and G6) U2OS cells transfected with shControl and shDNA-PKcs, respectively. The asterisk indicates nonspecific proteins recognized by the antibody. Tubulin was used as a loading control.

Published OnlineFirst September 9, 2019; DOI: 10.1158/1535-7163.MCT-18-1380

A

Treatment	No. of cells quantitated	% Interphase	% Mitotic	% Multinucleate	% Unscorable
Control					
24 h	626	96.0	3.2	0.8	0
48 h	560	96.1	3.4	0.5	0
72 h	926	89.7	1.3	0.6	8.3
CNDAC 0.5 μmol/L 24 h →					
No wash	858	95.9	3.1	0.8	0.1
Wash → 24 h	1,235	90.8	2.4	6.2	0.6
Wash → 48 h	947	86.9	1.4	4.8	7.0
CNDAC 1 μmol/L 24 h →					
No wash	669	95.2	2.2	2.2	0.3
Wash → 24 h	810	72.1	4.0	22.1	1.85
Wash → 48 h	832	78.6	1.3	12.7	7.3
CNDAC 10 μmol/L 24 h →					
No wash	605	96.9	0.5	2.6	0
Wash → 24 h	731	68.0	0	23.5	8.5
Wash → 48 h	792	43.8	3.8	34.1	18.3

B

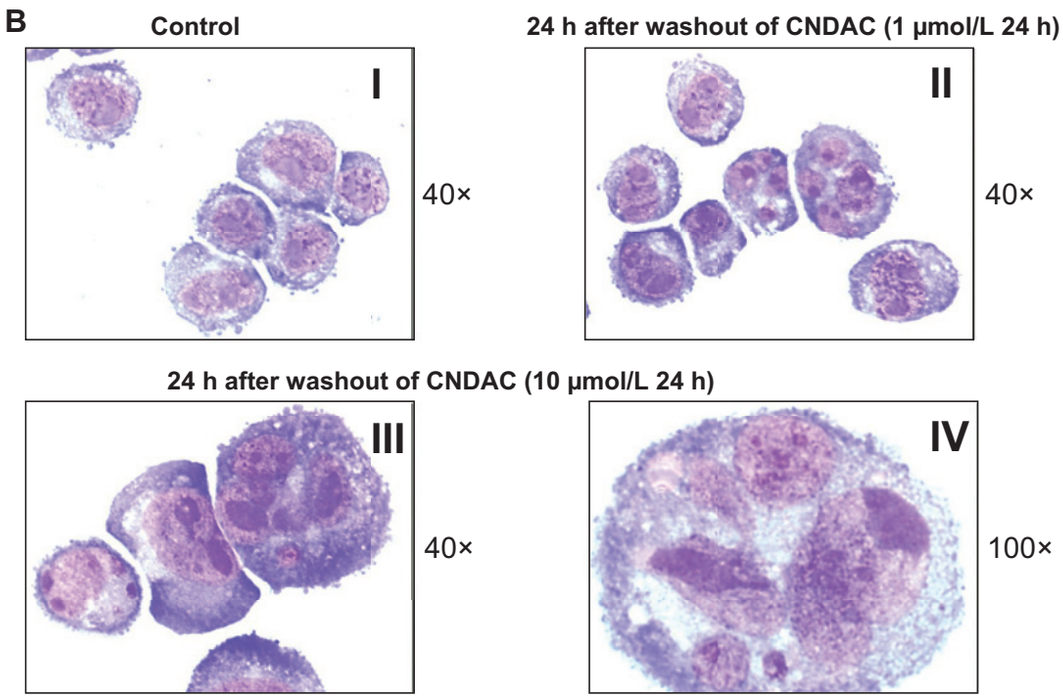

Figure 4.

Postmitosis nuclear alterations after washout of CNDAC: increase in multinucleated cells. AA8 cells were incubated with 0.5, 1, and 10 μmol/L CNDAC for 24 hours before washout and release into drug-free medium. Cells were detached without washing out of CNDAC, or 24 and 48 hours following washout. Cells were collected onto slides by cytospin, fixed, and stained with Giemsa. Nuclear morphologies of at least 600 cells were analyzed and categorized into interphase, mitotic, multinucleate, and unscorable. **A,** Quantitation of nuclear morphologies in cells following CNDAC washout. **B,** Representative images of Giemsa-stained AA8 cells. I, Control; II, 24 hours after washout of CNDAC (1 μmol/L 24 hours); III–IV, 24 hours after washout of CNDAC (10 μmol/L 24 hours). I–III, 40× objective; IV, 100× objective. No., number.

Published OnlineFirst September 9, 2019; DOI: 10.1158/1535-7163.MCT-18-1380

Live cell imaging reveals a prolonged second interphase, aberrant mitosis, and formation of multinucleate cells after CNDAC

Multi-nucleation, a hallmark of mitotic catastrophe, has been found in a significant portion of CNDAC-treated AA8 cells. We used time-lapse video microscopy to test the hypothesis that exposure of S-phase cells CNDAC causes mitotic catastrophe prior to cell death. The fate of AA8 cells stably transfected with a construct expressing H2B-GFP fusion protein after a 6-hour pulse 0.5, 1.0, and 10 μmol/L of CNDAC, respectively, was tracked followed by drug washout. Image capture was started immediately after wash. Cells entering the first mitosis within 5 hours after washout were presumed to have had CNDAC incorporation into DNA and therefore were eligible for analysis (Supplementary Fig. S5A). There was no difference in the duration of first mitosis among all three treatments and control (Fig. 5A–D, orange bars; Fig. 5E, $n \geq 24$, $P > 0.05$). However, the duration of second mitosis was significantly prolonged in a CNDAC concentration-dependent manner in all treatments compared with control (Fig. 5, red bars; Fig. 5E, $n \geq 37$, $P < 0.05$–0.001). The interval from the beginning of the first mitosis to the second was also prolonged markedly in 1 and 10 μmol/L CNDAC-treated samples (Fig. 5E, $P < 0.01$–0.001). A similar trend was observed in a H2B-GFP transfected H460 lung cancer cells following wash out of CNDAC (0.4 μmol/L, 8-hour exposure). In this case, because of the longer cell cycle time, cells entering first mitosis within 7.5 hours after wash were quantitated (Supplementary Fig. S5B). There was significant increase in the duration of second mitosis and in the interval between the first and second mitoses (Supplementary Fig. S6, $n \geq 38$, $P < 0.01$ and $P < 0.001$, respectively). Thus, cell-cycle progression was slowed due to CNDAC-induced DNA damage, especially when DSBs are expected to arise.

Notably, large numbers of CNDAC-treated AA8 cells were delayed in completion of the second mitosis, which was abnormal, and associated with the formation of multinucleate daughter cells (Fig. 5, blue bars). For cells exposed to 10 μmol/L CNDAC, multinucleation was found to be coupled to the second mitosis and followed by the onset of apoptosis in 18 out of 25 cells tracked. The snapshots in Fig. 6 and video clip in Supplementary Fig. S7 illustrate how one of those cells (#10) went through a seemingly normal, first mitosis (Fig. 6A), and its two daughter cells progressed through aberrant second mitoses followed by multinucleate formation and cell death (Fig. 6B). Multinucleation was also apparent in cells treated with different schedules of CNDAC exposure and washout (Supplementary Fig. S8). Thus, MM formation was frequently coupled with or followed by onset of apoptosis. Together the results from static nuclei (stained with Giemsa) and live cell imaging indicate that CNDAC-induced DSBs, which, if not repaired, trigger cells to undergo aberrant mitoses resulting in gross nuclear alterations. Multinucleation precedes eventual cell death through apoptosis, which was substantiated by cleavage of caspase-3 and PARP (Fig. 6C), as well as positive staining of Annexin V (Fig. 6D) after CNDAC washout. All the readouts showed concentration- and time-dependency.

Discussion

This study aimed at defining the mechanism by which CNDAC-induced DSBs lead to cell death. We used cytogenetic approaches to compare CNDAC-caused chromosomal damage in CHO cells proficient and deficient in XPF-ERCC1 nuclease. The increase in chromosomal aberrations after CNDAC exposure for an additional population doubling time (from one cell cycle to two cell cycles), regardless of XPF status, has provided direct cytogenetic evidence for conversion of CNDAC-induced SSBs into DSBs during DNA replication. Spontaneous chromosomal alterations in XPF-deficient cells were 7.6-fold greater than those in WT cells (Fig. 1A), indicating genetic instability conferred by XPF deficiency. The fold increase in chromosomal aberrations after CNDAC treatment was greater in *Xpf*-mutant than in WT cells, underlining the importance of XPF in repairing initial DNA damage caused by CNDAC. The XPF-ERCC1 endonuclease is multifunctional. It is not only essential for the NER pathway, but also for processing some blocked 3′ DNA ends, and for completing HR initiated by the Fanconi anemia pathway (19, 22, 23). XPF (ERCC4) has been identified as a Fanconi anemia factor, FANCQ (24). XPF-ERCC1 participates in the repair of interstrand crosslinks (ICL) by unhooking the crosslinks in concert with FANCD2 and FANCP/SLX4 (25). The resulting intermediate after resection is further processed by HR. Although both ERCC1 and XPF-mutant cells are sensitized by CNDAC (2.6- and 4.6-fold sensitization, respectively; ref. 9), we focused on XPF deficiency in the cytogenetic analysis and comet assay in the current study. In addition, the XPF-ERCC1 nuclease has been reported to facilitate Ku86-independent end joining of DSBs in yeast and mouse and human fibroblasts (26). Because XPF-ERCC1 can act to remove some blocks from the 3′ ends of DNA (such as 3′ deoxyribose-phosphate and 3′phosphoglycolate; ref. 27), it is likely that the enzyme may perform a similar reaction to excise CNddC, the *de facto* chain terminating lesion generated by β-elimination after incorporation of a deoxynucleotide following CNDACMP at the 3′ terminus of the DNA (6).

Thus, it is likely that XPF-ERCC1 nuclease contributes to the repair of the SSB caused by incorporation of CNDAC nucleotide into DNA. We have postulated that failure to repair nicked DNA may result in formation of a one-ended DSB upon a subsequent DNA replication cycle. Direct evidence for this was previously obtained by double labeling the DNA of ML-1 cells with a brief pulse of CNDAC and IdUrd (to mark the first S-phase) and followed by washing and addition of CldUrd before the second S-phase (8). Time-course flow cytometry demonstrated that entry of double positive cells into a second S-phase was concordant with DSB formation measured by pulse-field gel electrophoresis. The present studies are consistent with these findings in that they provide additional evidence of chromosome aberrations and DSB formation in the comet assay after two population-doubling times.

Besides the paired XPF cell lines, we chose to investigate cytogenetic alterations in RAD51D-deficient and proficient cells after CNDAC treatment as an indication for HR in the DNA damage repair processes. *RAD51D* mutations increase the risks for women to develop ovarian cancer (28, 29). Similar to XPF, deficiency in RAD51D renders genetic instability in that spontaneous chromosomal aberrations were more pronounced in AA8-derived cells lacking *Rad51D* (27% of the cell population) compared to cells complemented with *Rad51D* (10%, Fig. 2A). Both lines showed minimal cytogenetic changes (<4%) after one cell-cycle exposure to CNDAC, consistent with the timing of DSB induction by CNDAC after a second S-phase. After exposure for

Published OnlineFirst September 9, 2019; DOI: 10.1158/1535-7163.MCT-18-1380

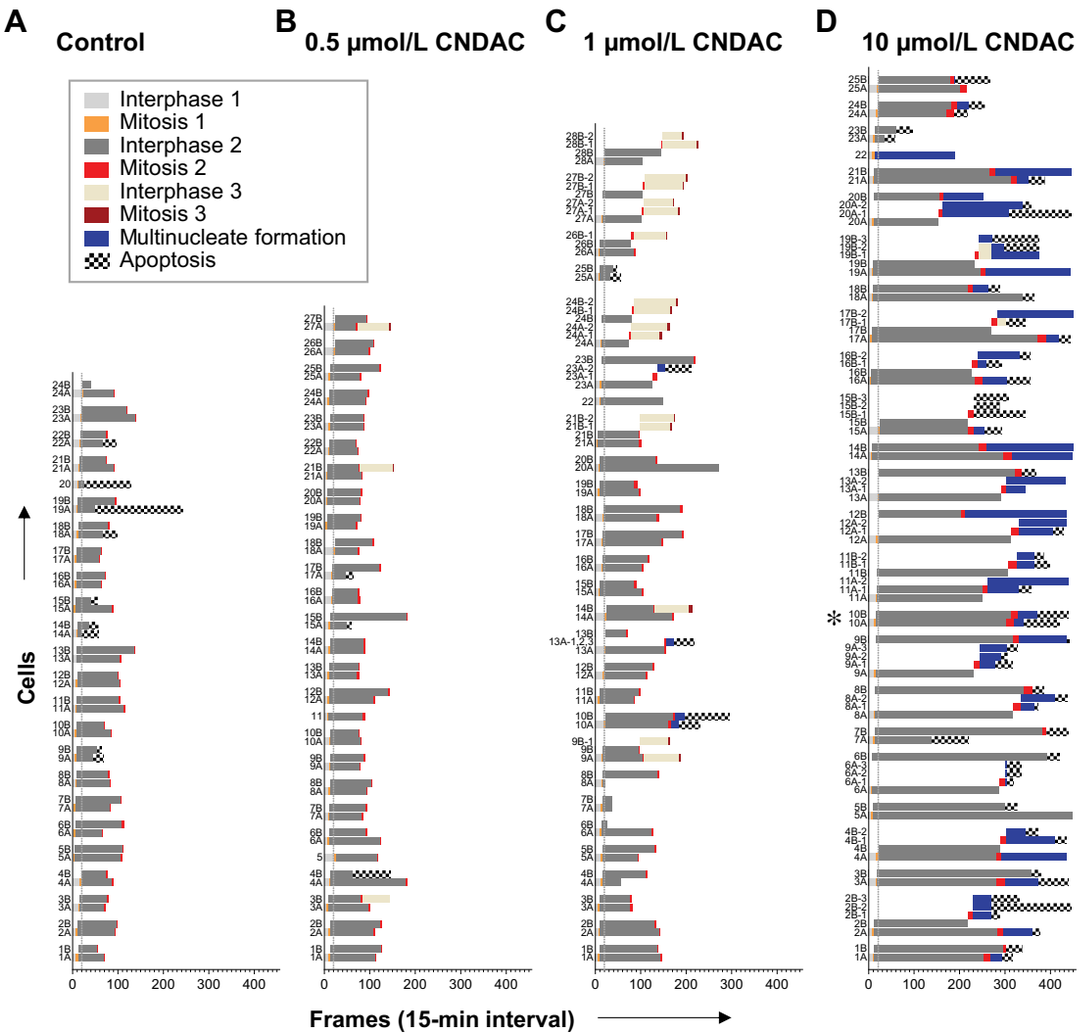

E

Treatment	1st Mitosis		2nd Mitosis		1st → 2nd Mitosis
Before washout	No. of cells tracked	Duration (min)	No. of daughter cells tracked	Duration (min)	Time (h)
Control	24	51.9 ± 10.8	37	52.3 ± 12.1	22.6 ± 5.0
0.5 μmol/L CNDAC	27	47.8 ± 8.4	49	58.5 ± 12.7 *	24.6 ± 6.9
1 μmol/L CNDAC	28	53 ± 7.6	44	69.9 ± 20.7 **	29.5 ± 7.8 **
10 μmol/L CNDAC	25	57.0 ± 15.0	40	200.3 ± 58.5 ***	66.5 ± 14.0 ***

*$P < 0.05$; **$P < 0.01$; ***$P < 0.001$

Figure 5.

Evidence from time-lapse video microscopy for CNDAC-triggered cell death through mitotic catastrophe. AA8/H2B-GFP cells were treated with 0.5, 1, and 10 μmol/L CNDAC, respectively, for 6 hours before release into drug-free medium. Cells were monitored for approximately 5 days (114 hours) after washout. A minimum of 24 cells entering mitosis within the beginning 20 frames, equivalent to 5 hours, were analyzed. Contingency bar plots of control cells (**A**) and CNDAC-treated cells, 0.5 μmol/L (**B**), 1 μmol/L (**C**), and 10 μmol/L (**D**), are shown. Color bars represent the first to third interphases, the first to third mitoses, and the phases of multinucleate formation and apoptosis, respectively. **D,** The asterisk symbol (*) indicates the particular daughter cells tracked in Fig. 6. **E,** Quantitation and statistical analysis of time-lapse video microscopy: duration of mitoses and intervals between the first and second mitoses after CNDAC washout. No., number.

Published OnlineFirst September 9, 2019; DOI: 10.1158/1535-7163.MCT-18-1380

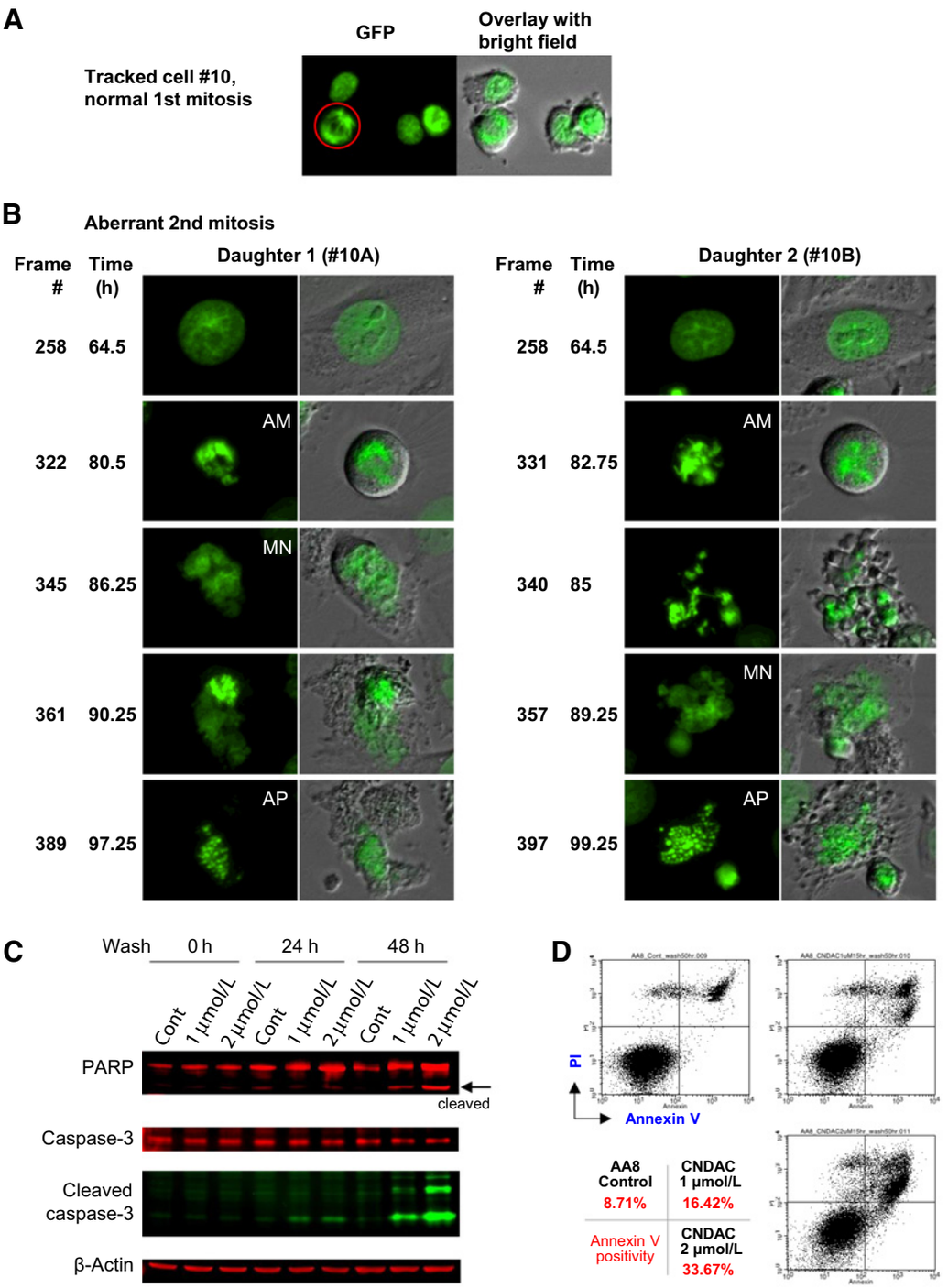

Figure 6.

Evidence from time-lapse video microscopy for CNDAC-triggered cell death through mitotic catastrophe. Snapshots of representative AA8 cells undergoing aberrant mitosis (AM), multinucleate formation (MN), and apoptosis (AP) are shown. **A,** Fluorescent (GFP) image and its overlay with brightfield of the particular cell tracked (#10 in Fig. 4D), taken 3.25 hours after CNDAC washout (Frame 13). **B,** Fluorescent images of the two daughter cells (#10A and #10B in Fig. 5D) and corresponding overlays with bright field, taken at indicated frames and equivalent times. **C,** Immunoblotting of PARP and caspase-3, both in noncleaved and cleaved forms, in AA8 cells washed 24 and 48 hours, respectively, after incubation with 1 and 2 μmol/L CNDAC for 15 hours. β-Actin was used as a loading control. **D,** AA8 cells, treated as in **C** and incubated for 50 hours after CNDAC washout, were subjected to staining with Annexin V and propidium iodide (PI), followed by detection with flow cytometry. Percentage of Annexin V positively stained population was indicated for each treatment.

Published OnlineFirst September 9, 2019; DOI: 10.1158/1535-7163.MCT-18-1380

two cell cycles, the vast majority of RAD51D repleted cells (99%) could be analyzed, whereas only a minor portion of RAD51D-deficient cells (24%) were scorable, as most cells had extensive chromosome damage (Fig. 2A). This further highlighted the significance of RAD51D and the HR pathway in repair of CNDAC-induced DSBs. The finding that cells lacking HR components such as RAD51D cause significantly more chromosomal aberrations and greater clonogenic sensitization to CNDAC than XPF mutant cells, supports the conclusion that the chromosomal alterations in XPF deficient cells in response to CNDAC are mainly due to an HR-independent function of XPF-ERCC1.

Investigations with the *Polq* (or *POLQ*) knockout cell lines indicated that the absence of Pol θ function (30) does not sensitize cells to CNDAC as measured by clonogenic survival (Fig. 3; refs. 6, 31). Thus, it is unlikely that the alternative DNA end-joining pathway has a crucial role in repair of CNDAC-induced DSBs. Considering that deficiency in the classical NHEJ pathway (deficiency in either DNA-PKcs or Ku80) does not confer sensitivity to CNDAC, homologous recombination is indeed the major mechanism for the repair of CNDAC-induced DSBs (8).

Furthermore, we employed a traditional method, Giemsa staining of AA8 cells treated with and then washed out of CNDAC, to demonstrate the presence of multinucleate cells, which is indicative of aberrant mitosis and characteristic of mitotic catastrophe (32). To detect relatively low levels of DNA damage in repair competent cells, we treated cells with lesser concentrations of CNDAC (0.5 and 1 μmol/L) and a greater concentration (10 μmol/L) that delayed cell-cycle progression. The percentage of multi-nucleated cells was dependent upon both CNDAC concentration and length of exposure time. Interestingly, multinucleate cells became discernible only after two PDTs, highlighting that a second mitosis is needed to enable the aberrant nuclear alterations to occur and accumulate.

Finally, we exploited time-lapse video microscopy to better observe cells in real time and verify mitotic catastrophe occurrence after CNDAC exposure and washout. The GFP-tagged histone H2B stable expressing system was used to monitor long-term dynamics of nuclei and chromosomes without compromising their structures (33). Live cell imaging of two cell lines of distinct origins demonstrated that conditions that cause CNDAC-induced DSBs trigger cells to undergo an extended interphase followed by a prolonged second mitosis, coupled with multinucleation and subsequent apoptosis. Such a process characterizes mitotic catastrophe, which is visualized by the multinucleate formation after an aberrant attempt at mitosis, and is regarded as an oncosuppressive process for maintaining genomic stability by leading to apoptosis, senescence, or necrosis (34). Active cancer therapeutics that damage DNA integrity or interfere with mitotic processes are known to induce mitotic catastrophe (35). The demonstration of multinucleate cells following CNDAC treatment suggests the possibility that this may serve as a pharmacodynamic indicator in clinical trials. This possibility may be evaluated in clinical trials of the parenteral formulation of CNDAC (as DFP-10917) or of sapacitabine, the orally bioavailable prodrug of CNDAC, which are undergoing clinical trials in AML and myelodysplastic syndromes with encouraging outcomes (2–4, 36). Furthermore, sapacitabine has also shown antitumor activities in multiple solid tumor types lacking BRCA1 or BRCA2 (37, 38), confirming our findings in hamster and human cell lines (8, 39).

Disclosure of Potential Conflicts of Interest

R.D. Wood is a scientific advisory board member for Repare Therapeutics. No potential conflicts of interest were disclosed by the other authors.

Authors' Contributions

Conception and design: X. Liu, W. Plunkett
Development of methodology: X. Liu, Y. Jiang, K. Takata, R.D. Wood, W.N. Hittelman
Acquisition of data (provided animals, acquired and managed patients, provided facilities, etc.): X. Liu, Y. Jiang, K. Takata, B. Nowak, C. Liu, R.D. Wood, W.N. Hittelman
Analysis and interpretation of data (e.g., statistical analysis, biostatistics, computational analysis): X. Liu, Y. Jiang, K. Takata, W.N. Hittelman, W. Plunkett
Writing, review, and/or revision of the manuscript: X. Liu, Y. Jiang, K. Takata, R.D. Wood, W.N. Hittelman, W. Plunkett
Administrative, technical, or material support (i.e., reporting or organizing data, constructing databases): X. Liu, Y. Jiang, B. Nowak
Study supervision: W. Plunkett

Acknowledgments

This work was supported by grant R01 CA28596 (to W. Plunkett) and Cancer Center Support grant P30 CA16672 from the NCI, Department of Health and Human Services. R.D. Wood was supported by NIH P01 grant CA193124 and the Grady F. Saunders, PhD Distinguished Research Professorship. K. Takata was supported by an Institutional Research Grant (IRG) from The University of Texas MD Anderson Cancer Center and by the Center for Radiation Oncology Research (CROR). We thank Drs. Simona Colla and Andrea Santoni for their assistance with Comet Assay IV software.

The costs of publication of this article were defrayed in part by the payment of page charges. This article must therefore be hereby marked *advertisement* in accordance with 18 U.S.C. Section 1734 solely to indicate this fact.

Received December 21, 2018; revised June 14, 2019; accepted September 4, 2019; published first September 9, 2019.

References

1. Kantarjian HM, Jabbour EJ, Garcia-Manero G, Kadia TM, DiNardo CD, Daver NG, et al. Phase 1/2 study of DFP-10917 administered by continuous intravenous infusion in patients with recurrent or refractory acute myeloid leukemia. Cancer 2019;125:1665–73.
2. Kantarjian H, Garcia-Manero G, O'Brien S, Faderl S, Ravandi F, Westwood R, et al. Phase I clinical and pharmacokinetic study of oral sapacitabine in patients with acute leukemia and myelodysplastic syndrome. J Clin Oncol 2010;28:285–91.
3. Kantarjian H, Faderl S, Garcia-Manero G, Luger S, Venugopal P, Maness L, et al. Oral sapacitabine for the treatment of acute myeloid leukaemia in elderly patients: a randomised phase 2 study. Lancet Oncol 2012;13:1096–104.
4. Kantarjian HM, Begna KH, Altman JK, Goldberg SL, Sekeres MA, Strickland SA, et al. Results of a phase 3 study of elderly patients with newly diagnosed AML treated with sapacitabine and decitabine administered in alternating cycles. Blood 2017;130 Suppl 1:891.
5. Liu X, Kantarjian H, Plunkett W. Sapacitabine for cancer. Expert Opin Investig Drugs 2012;21:541–55.
6. Azuma A, Huang P, Matsuda A, Plunkett W. 2′-C-cyano-2′-deoxy-1-beta-D-arabino-pentofuranosylcytosine: a novel anticancer nucleoside analog that

causes both DNA strand breaks and G(2) arrest. Mol Pharmacol 2001;59:725–31.
7. Hanaoka K, Suzuki M, Kobayashi T, Tanzawa F, Tanaka K, Shibayama T, et al. Antitumor activity and novel DNA-self-strand-breaking mechanism of CNDAC (1-(2-C-cyano-2-deoxy-beta-D-arabino-pentofuranosyl) cytosine) and its N4-palmitoyl derivative (CS-682). Int J Cancer 1999;82:226–36.
8. Liu X, Wang Y, Benaissa S, Matsuda A, Kantarjian H, Estrov Z, et al. Homologous recombination as a resistance mechanism to replication-induced double-strand breaks caused by the antileukemia agent CNDAC. Blood 2010;116:1737–46.
9. Wang Y, Liu X, Matsuda A, Plunkett W. Repair of 2′-C-cyano-2′-deoxy-1-beta-D-arabino-pentofuranosylcytosine-induced DNA single-strand breaks by transcription-coupled nucleotide excision repair. Cancer Res 2008;68:3881–9.
10. Abo MA, Sasanuma H, Liu X, Rajapakse VN, Huang SY, Kiselev E, et al. TDP1 is critical for the repair of DNA breaks induced by sapacitabine, a nucleoside also targeting ATM- and BRCA-deficient tumors. Mol Cancer Ther 2017;16:2543–51.
11. Yousefzadeh MJ, Wyatt DW, Takata K, Mu Y, Hensley SC, Tomida J, et al. Mechanism of suppression of chromosomal instability by DNA polymerase POLQ. PLoS Genet 2014;10:e1004654.
12. Ceccaldi R, Liu JC, Amunugama R, Hajdu I, Primack B, Petalcorin MI, et al. Homologous-recombination-deficient tumours are dependent on Pol theta-mediated repair. Nature 2015;518:258–62.
13. Mateos-Gomez PA, Kent T, Deng SK, McDevitt S, Kashkina E, Hoang TM, et al. The helicase domain of Poltheta counteracts RPA to promote alt-NHEJ. Nat Struct Mol Biol 2017;24:1116–23.
14. Liu X, Guo Y, Li Y, Jiang Y, Chubb S, Azuma A, et al. Molecular basis for G2 arrest induced by 2′-C-cyano-2′-deoxy-1-beta-D-arabino-pentofuranosylcytosine and consequences of checkpoint abrogation. Cancer Res 2005;65:6874–81.
15. Matsuda A, Nakajima Y, Azuma A, Tanaka M, Sasaki T. Nucleosides and nucleotides. 100. 2′-C-cyano-2′-deoxy-1-beta-D-arabinofuranosylcytosine (CNDAC): design of a potential mechanism-based DNA-strand-breaking antineoplastic nucleoside. J Med Chem 1991;34:2917–9.
16. Azuma A, Nakajima Y, Nishizono N, Minakawa N, Suzuki M, Hanaoka K, et al. Nucleosides and nucleotides. 122. 2′-C-cyano-2′-deoxy-1-beta-D-arabinofuranosylcytosine and its derivatives. A new class of nucleoside with a broad antitumor spectrum. J Med Chem 1993;36:4183–9.
17. Hinz JM, Tebbs RS, Wilson PF, Nham PB, Salazar EP, Nagasawa H, et al. Repression of mutagenesis by Rad51D-mediated homologous recombination. Nucleic Acids Res 2006;34:1358–68.
18. Kanda T, Sullivan KF, Wahl GM. Histone-GFP fusion protein enables sensitive analysis of chromosome dynamics in living mammalian cells. Curr Biol 1998;8:377–85.
19. Manandhar M, Boulware KS, Wood RD. The ERCC1 and ERCC4 (XPF) genes and gene products. Gene 2015;569:153–61.
20. Talbert LL, Coletta LD, Lowery MG, Bolt A, Trono D, Adair GM, et al. Characterization of CHO XPF mutant UV41: influence of XPF heterozygosity on double-strand break-induced intrachromosomal recombination. DNA Repair 2008;7:1319–29.
21. Takata M, Sasaki MS, Tachiiri S, Fukushima T, Sonoda E, Schild D, et al. Chromosome instability and defective recombinational repair in knockout mutants of the five Rad51 paralogs. Mol Cell Biol 2001;21:2858–66.
22. Al-Minawi AZ, Lee YF, Hakansson D, Johansson F, Lundin C, Saleh-Gohari N, et al. The ERCC1/XPF endonuclease is required for completion of homologous recombination at DNA replication forks stalled by inter-strand cross-links. Nucleic Acids Res 2009;37:6400–13.
23. Kikuchi K, Narita T, Pham VT, Iijima J, Hirota K, Keka IS, et al. Structure-specific endonucleases xpf and mus81 play overlapping but essential roles in DNA repair by homologous recombination. Cancer Res 2013;73:4362–71.
24. Ceccaldi R, Sarangi P, D'Andrea AD. The Fanconi anaemia pathway: new players and new functions. Nat Rev Mol Cell Biol 2016;17:337–49.
25. Klein Douwel D, Boonen RA, Long DT, Szypowska AA, Raschle M, Walter JC, et al. XPF-ERCC1 acts in Unhooking DNA interstrand crosslinks in cooperation with FANCD2 and FANCP/SLX4. Mol Cell 2014;54:460–71.
26. Ahmad A, Robinson AR, Duensing A, van Drunen E, Beverloo HB, Weisberg DB, et al. ERCC1-XPF endonuclease facilitates DNA double-strand break repair. Mol Cell Biol 2008;28:5082–92.
27. Fisher LA, Samson L, Bessho T. Removal of reactive oxygen species-induced 3′-blocked ends by XPF-ERCC1. Chem Res Toxicol 2011;24:1876–81.
28. Loveday C, Turnbull C, Ramsay E, Hughes D, Ruark E, Frankum JR, et al. Germline mutations in RAD51D confer susceptibility to ovarian cancer. Nat Genet 2011;43:879–82.
29. Osher DJ, De Leeneer K, Michils G, Hamel N, Tomiak E, Poppe B, et al. Mutation analysis of RAD51D in non-BRCA1/2 ovarian and breast cancer families. Br J Cancer 2012;106:1460–3.
30. Zahn KE, Averill AM, Aller P, Wood RD, Doublie S. Human DNA polymerase theta grasps the primer terminus to mediate DNA repair. Nat Struct Mol Biol 2015;22:304–11.
31. Yousefzadeh MJ, Wood RD. DNA polymerase POLQ and cellular defense against DNA damage. DNA Repair 2013;12:1–9.
32. Galluzzi L, Vitale I, Aaronson SA, Abrams JM, Adam D, Agostinis P, et al. Molecular mechanisms of cell death: recommendations of the Nomenclature Committee on Cell Death 2018. Cell Death Differ 2018;25:486–541.
33. Ettinger A, Wittmann T. Fluorescence live cell imaging. Methods Cell Biol 2014;123:77–94.
34. Vitale I, Galluzzi L, Castedo M, Kroemer G. Mitotic catastrophe: a mechanism for avoiding genomic instability. Nat Rev Mol Cell Biol 2011;12:385–92.
35. Mc Gee MM. Targeting the mitotic catastrophe signaling pathway in cancer. Mediators Inflamm 2015;2015:146282.
36. Kantarjian HM, Jabbour EJ, Garcia-Manero G, Kadia TM, DiNardo CD, Daver NG, et al. Phase I/II study of DFP-10917 in relapsed/refractory AML demonstrates efficacy and safety profile suitable for phase III study. Blood 2016;128:2822.
37. Shapiro GI, Hilton J, Cleary JM, Tolaney SM, Ghandi L, Kwak EL, et al. Responses to sequential sapacitabine and seliciclib in patients with brca-deficient solid tumors. In: Proceedings of the 104th Annual Meeting of the American Association for Cancer Research; 2013 Apr 6–10; Washington, DC. Philadelphia (PA): AACR; 2013. Abstract nr LB-202.
38. Tolaney SM, Hilton JF, Cleary JM, Ghandi L, Kwak EL, Clark JW, et al. Phase I study of sapacitabine and seliciclib in patients with advanced solid tumors. J Clin Oncol 2016;34 Suppl 15:2503.
39. Liu X, Jiang Y, Nowak B, Qiang B, Cheng N, Chen Y, et al. Targeting BRCA1/2 deficient ovarian cancer with CNDAC-based drug combinations. Cancer Chemother Pharmacol 2018;81:255–67.

Published OnlineFirst September 9, 2019; DOI: 10.1158/1535-7163.MCT-18-1380

Molecular Cancer Therapeutics

CNDAC-Induced DNA Double-Strand Breaks Cause Aberrant Mitosis Prior to Cell Death

Xiaojun Liu, Yingjun Jiang, Kei-ichi Takata, et al.

Mol Cancer Ther 2019;18:2283-2295. Published OnlineFirst September 9, 2019.